# DESIGN AND PERFORMANCE TEST OF PLOWING AND ROTARY TILLAGE COMBINED MACHINE

# /

# 秸秆犁翻旋整联合作业机的设计及试验

**Bao Xuanbin [1)], Zhao Xiangyu [1)], He Jin [*1)], Li Hongwen[1)], Wang Qingjie[1)], Liu Wenzheng[1)], [1]**

[1)]College of Engineering, China Agricultural University, Beijing/China

*Tel: 8610 62737300; E-mail: hejin@cau.edu.cn*

*DOI: 10.35633/INMATEH-58-23*

***Key words:*** *combined machine, straw burying, Discrete Element, rotary tiller*

**ABSTRACT**

*Straw returning is an effective option to avoid straw open burning during harvest seasons and has been widely implemented all over the world. This study developed a plowing and rotary tillage combined machine, which could bury the straw, break the soil and prepare the soil for planting in one operation. The machine consists of plowing component, rotary component and power transmission system. The plow component was designed by the response surface analysis, which analyzed the influence of different contour line of plow surface on the burying effect and the working resistance at the speeds of 0.8m/s, 1.0m/s and 1.2m/s respectively. In combination with the working effect of the plow component, the rotary blades were arranged by the method of 4n±2. The orthogonal test results showed that the C-plow surface has the best burying effect at 1m/s. The field tests showed that the machine had a straw burying rate of 91%, surface roughness was 0.564, fuel consumption was 43.41 kg/ha and the soil-breaking rate reached 96.08%; all the performance indexes met the design requirements. The study can provide theoretical reference for parameters design of plowing and rotary tillage combined machine.*

**摘要**

*作物秸秆还田是避免秸秆露天焚烧的一种有效途径，在全球已经广泛应用。本文设计了一种秸秆犁翻旋整联合作业机，一次下地作业就可完成秸秆翻埋、碎土、整地等多道作业工序。机具主要由犁翻部件、旋整部件和传动系统组成。犁翻部件的设计基于对不同犁体曲面在 0.8m/s、1.0m/s 和 1.2m/s 的速度下犁翻部件翻埋效果及作业阻力进行响应面法分析。结合犁翻部件的作业效果，旋整刀采用 4n±2 的方式进行排列。正交试验结果表明，犁体曲面 C 在 1m/s 的作业速度下达到最好翻埋效果。田间试验表明，该机具的秸秆翻埋率为 91%，土壤粉碎率为 96.08%，地表平整度为 0.564，稳定作业油耗为每公顷 43.41 千克，所有性能指标均满足设计要求。本文的研究结果为秸秆犁翻旋整联合作业机参数的设计提供了理论参考。*

## INTRODUCTION

With the improvements in varieties, farming technologies and pest management, a high quantity of straw residues will be produced proportionally *(Chang et al., 2014)*. Large amount of straw residues drives local famers to burn them directly in open fields *(Yang et al., 2018)*. Straw contains abundant organic matters, potassium, phosphorous, nitrogen and other trace elements, which is considered to be desirable fertilizer for crop growth *(Li et al., 2018)*. Many studies conducted to the fact that the straw returning in the soil is beneficial for the improvement of soil properties and crop productivity *(Zeng et al., 2002; Zeng et al., 2007)*.

Both the straw plowing and rotary tillage are important components of straw returning. The current research on mouldboard plow is mainly to increase the width and speed of plowing operation, which could improve the work efficiency *(Xie et al., 2009)*. LEMKEN's semi-mounted hitch two-way moldboard plows (Euro Titan) have 9-12 bottoms and each bottom has a working width of 30-55 cm and a spacing of 100 cm. In China, it is mainly to reduce the resistance and improve the quality of tillage in order to achieve better tillage operation with low fuel consumption. The development direction of rotary tiller is large width *(Jia et al., 2007)*, high speed and deep tillage with the improvement of tractor power. The PANTRRA-620 rotary tiller produced by Maschio has a working width of 628cm and a depth of 29cm.

---

[1] *Bao Xuanbin, M.D. Stud.; Zhao Xiangyu, M.D.; He Jin, Prof.; Li Hongwen, Prof.; Wang Qingjie, Prof.; Liu Wenzheng, Ph.D. Stud.*

For the currently widely used plowing and rotary tillage operation, a moldboard plow is often first used to bury straw in the soil. Then a rototiller is used to shallowly rototill the soil to mix part of the straw with the soil and meet the requirements of preparation of soil before planting. However, the single-purpose moldboard plow and rototiller have some drawbacks. After the plowing operation, a rototiller is also needed to prepare the soil for planting, resulting in soil compaction and increasing operating costs. Otherwise, the theoretical research and experimental proof of the interaction between the matching design, the straw burying effect and the drag reduction effect are still omitted.

To overcome the drawbacks of these two kinds of machines, this study developed a plowing and rotary tillage combined machine, which can bury the straw, break the soil and prepare the soil for planting simultaneously. This paper described the working principle and structural features of the combined machine, the design of the working components for straw burying and rototilling. Field test results were also presented and discussed.

## DESIGN OF PLOWING AND ROTARY TILLAGE COMBINED MACHINE

### Working principle

Plowing and rotary tillage combined machine (Fig.1) consisted of plowing component, rotary component and power transmission system. The machine adopted the mounted method of three-point integral and arranged in the sequence of plowing and rotary component. The power from the tractor was transferred to the gearbox via the power take-off shaft and then drove the blade rotors.

When the machine operated, the plowing component firstly plowed the surface covered by the straw and initially completed the turning of the soil and the burying of the straw. Then rotary component further completed the smashing and the preparation of the soil. The main technical parameters of the machine were shown in Table 1.


**Fig. 1 - Structural scheme of the combined machine**

*1 - Plowing component; 2 - power transmission system; 3 - rotary components*

**Table 1**

**Main technical parameters of plowing and rotary tillage combined machine**

| Parameters | value | Parameters | value |
|---|---|---|---|
| Matched power [kW] | ≥65 | Productivity [ha/h] | ≥0.4 |
| Working width [mm] | 2500 | Plowing depth [mm] | 250-300 |
| Bottom number | 5 | Rotation depth [mm] | 100-150 |

### Design of the plowing component

The design of plowing component consisted of the design of plow surface and simulation analysis. According to the technical parameter requirements of the plowing and rotary tillage combined machine, the width of the plowing component should be less than 2500 mm to ensure no missing and no repeated tillage when the width of rotary component is 2500 mm.

The length of the frame was determined by the longitudinal spacing of the plow body. As shown in Fig.2, $L$ is the longitudinal spacing of the plow component, calculated as followed:

$$L = b \times \tan(\theta_0 + \varphi) \quad (1)$$

where:

$b$ is the width of the moldboard plow;

$\theta_0$ is the angle between the plow line and the forward direction;

$\varphi$ is the friction angle between soil and steel.

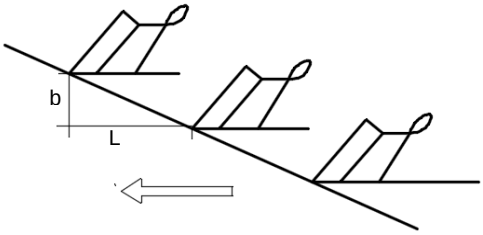


**Fig. 2 - Schematic of plow components' longitudinal spacing**

Therefore, the longitudinal spacing *L* of the plow was 692 mm and the length of the plow components' frame was 2400 mm.

The straw burying was directly affected by the plowing surface. Based on the existing design parameters of plow surface (Table.2), a mathematical model was established by horizontal straight-line elements (HSE).

**Table 2**

**Basic design parameters of plow surface**

| Parameters of plow surface | Value |
|---|---|
| Working width *b* [mm] | 450 |
| Plowing depth *a* [mm] | 300 |
| Height of the plow surface $h_{max}$ [mm] | 495 |
| Bottom installation angle $\varepsilon$ [°] | 25 |
| Length of the beginning line *S* [mm] | 50 |
| Plow surface tangential angle $\omega$ [°] | 110 |
| HSE angles of plow surface $\theta_0$, $\theta_{min}$, $\theta_{max}$ [°] | 36, 34, 45 |

***Determination of horizontal straight-line element angles of plow surface***

The calculation of each HSE angle of the plow surface was divided into two sections. The first section was $\theta_0$ to $\theta_{min}$ and the change of HSE angle was linear. The second section was $\theta_{min}$ to $\theta_{max}$, and the change of HSE angle was non-linear quadratic function (Fig.3).

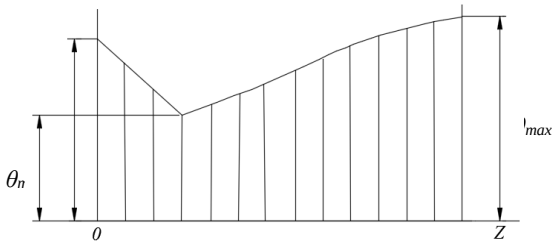


**Fig. 3 - Diagram of element line angle change**

From $\theta_0$ to $\theta_{min}$, the HSE angle changed linearly, and each HSE angle $\theta_{n1}$ was calculated by equation 2:

$$\begin{cases} \theta_{n1} = \theta_0 + K \times Z(n_1) \\ K = \dfrac{\theta_{\min} - \theta_0}{Z_{\min}} \end{cases} \quad (2)$$

where:

$\theta_{n1}$ is the angle of each HSE;

*K* is the slope of $\theta_0$ to $\theta_{min}$ section;

$Z(n_1)$ is the height of the n-th HSE of the plow surface.

From $\theta_{min}$ to $\theta_{max}$, the change of each HSE angle $\theta_{n2}$ is shown as equation (3). All the HSE angles of the plow surface are shown in Table 3.

$$\theta_{n2} = \theta_{\min} + \frac{(\theta_{\max} - \theta_{\min}) \times (Z(n_2) - Z_{\min})^2}{(Z_{\max} - Z_{\min})^2} \quad (3)$$

where:

$\theta_{n1}$ is the angle of each straight-line element;

$Z(n_2)$ is the height of the n-th HSE of the plow surface.

**Table 3**

**The horizontal straight-line element angles of the plow surface**

| | Number of the HSE / N | HSE angle / θ | Number of HSE / N | HSE angle / θ |
|---|---|---|---|---|
| $\theta_{n1}$ | 0 | 36° | 2 | 34.67° |
| | 1 | 35.33° | 3 | 34° |
| $\theta_{n2}$ | 4 | 34.04° | 12 | 37.48° |
| | 5 | 34.17° | 13 | 38.30° |
| | 6 | 34.39° | 14 | 39.20° |
| | 7 | 34.69° | 15 | 40.19° |
| | 8 | 35.07° | 16 | 41.26° |
| | 9 | 35.55° | 17 | 42.42° |
| | 10 | 36.11° | 18 | 43.67° |
| | 11 | 36.75° | 19 | 45° |

***Determination of plow guiding curve***

The plow guiding curve was mainly composed by the straight-line portion (S) and the curved portion (Q) (Fig.4). The points (O), (B) and (E) were the origin, vertex and intersection point of the guiding curve, respectively and the two tangent lines intersected at the point (E). The straight line (OE) portion and the straight line (BE) portion were defined as (I) and (II) respectively. According to the basic design parameters of plow surface in Table 2, the equations of the straight line (I) and (II) were determined as followed:

(I): $$z = x \times \tan\varepsilon = 0.47x \quad (4)$$

(II): $$z = h_{\max} - (x - L) \times \tan(\omega - \varepsilon) = 4266.9 - 11.43x \quad (5)$$

where:

$\varepsilon$ is the rake angle of plow surface;

$h_{max}$ is the maximum height of the top edge line of the plow surface;

$L$ is the opening of guiding curve;

$\omega$ is the angle between the tangent of the upper and lower endpoints of plow guiding curve.

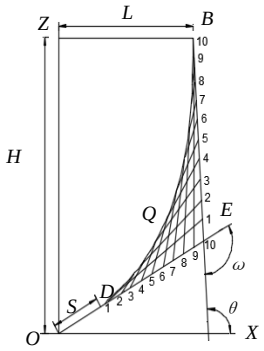


**Fig. 4 - Diagram of plow guiding curve**

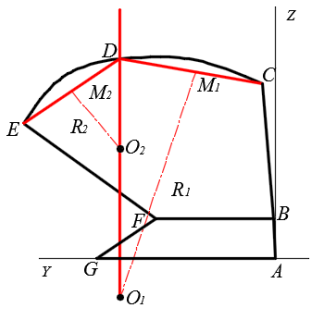


**Fig. 5 - Projection of the plow surface on the ZOY plane**

From the diagram of plow guiding curve, the coordinate of the end point of the S was D ($S\times\cos\varepsilon$, $S\times\sin\varepsilon$) and the vertex coordinate of the Q portion was B ($L$, $h_{max}$). Substituting the known parameters, the coordinate of D and B were (45.32, 21.13) and (330, 495), respectively. Combining equation (4) with equation (5) the coordinate of point E was obtained:

$$\begin{cases} z_E = x_E \tan\varepsilon \\ x_E = \dfrac{h_{\max} + L\tan(\omega - \varepsilon)}{\tan(\omega - \varepsilon) + \tan\varepsilon} \end{cases} \quad (6)$$

The guiding curve was drawn by the envelope method. The straight line (I) and (II) in the diagram of plow guiding curve were equally divided into m parts, m=10. The coordinates of the j-th points on the straight lines (I) and (II) were obtained by equation (7).

$$\text{I}\begin{cases} DE_{x(j)} = x_D + j \times \dfrac{x_E - x_D}{m} \\ DE_{z(j)} = z_D + j \times \dfrac{z_E - z_D}{m} \end{cases} \qquad \text{II}\begin{cases} BE_{x(j)} = x_D - j \times \dfrac{x_E - x_B}{m} \\ BE_{z(j)} = z_D - j \times \dfrac{z_E - z_B}{m} \end{cases} \quad (7)$$

The points on the straight lines (I) and (II) in the guiding curve were connected correspondingly to form m straight lines. The n-th HSE intersected the *m* straight lines to form *m* intersection points. The abscissa of the intersection obtained by the HSE with the j-th line was calculated from equation (8). The minimum of the m abscissa values was the guiding curve opening of the n-th HSE, which was denoted as *K(n)*, and the coordinate of the intersection was (*K(n)*, *Z(n)*). The curve portion Q of plow guiding curve was obtained by connecting the opening values *K(n)* with a smooth curve. The curve portion Q and the straight portion S formed the plow guiding curved.

$$X\left(n,j\right)=DE_{x(j)}+\left(N\times\Delta H-DE_{y(j)}\right)\times\frac{BE_{x(j)}-DE_{x(j)}}{BE_{y(j)}-DE_{y(j)}} \quad (8)$$

***Establishment of plow surface simulation model***

Using the intersection coordinates of the HSE and the plow surface's projection in the ZOY plane (Fig.5), Y-axis range of each HSE was determined under different Z-axis. In the operation, the final working part of the plow surface on the straw and soil was moldboard. The length of the moldboard was determined by the intersection E of the moldboard line (EF) and the top edge line (DE). By changing coordinate of the point E in the Z-axis, different plow surface contour lines were formed.

In this study, three plow surfaces were designed (Fig.6). The three plow surfaces parameters were same except the Z-axis value of the intersection point (the side line (EF) and the top edge line (DE) of the plow surface). Table 4 shows the specific parameters of the three plow surfaces.

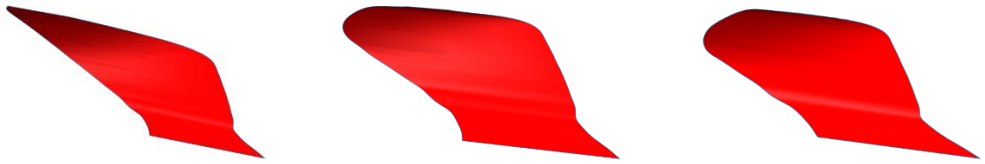

*A-plow surface* *B-plow surface* *C-plow surface*

**Fig. 6 - Three kinds of plow surfaces**

**Table 4**

**Three plow surface parameters**

| **Type of plow surface** | A | B | C | Other parameters are shown in Table 2. |
|---|---|---|---|---|
| **Z-axis Value [mm]** | 468 | 442 | 416 | |

***Simulation analysis of plow surface***

By simulating different intersection positions of moldboard line and top edge line on plow surface in different speeds, the influence on working resistance and turning effect of plow surface was analyzed. And the optimal combination to determine the plow surface was selected. The following parameters (Table 5) were measured by the soil parameter calibration test *(Kornei et al., 2013; Ucgul M. et al., 2014; Lenaerts B. et al., 2014; Zheng and He et al., 2016)*.

**Table 5**

**Partial parameters of soil and plow surface**

| **Parameters** | **Value** | **Parameters** | **Value** |
|---|---|---|---|
| Clay soil particles | 56.67% | Static friction coefficient | 0.33 |
| Recovery coefficient between particles | 0.6 | Static friction coefficient between soil particles and the plow surface | 0.42 |
| Rolling friction coefficient between particles | 0.17 | Rolling friction coefficient between soil particles and the plow surface | 0.05 |

Therefore, the soil particle model and straw particle coverage model were established (Fig. 7a). The straw particle coverage model was built based on the mass of straw per unit area. Furthermore, the straw particle model was simplified as a cylindrical type consisting of three particles with radius of 10 mm (Fig. 7b).

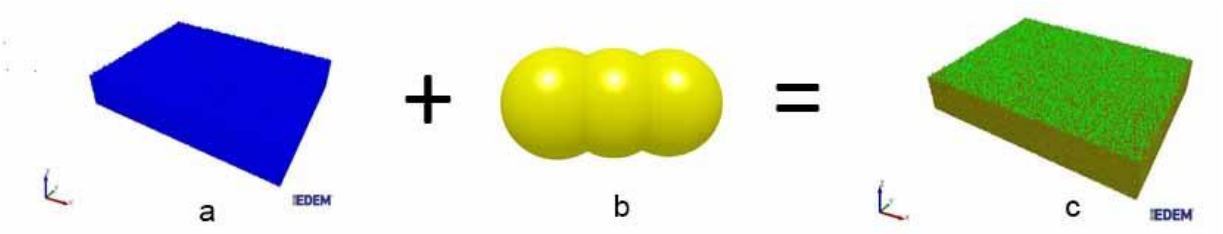


**Fig. 7 - Straw covered soil trough EDEM simulation model**

*a - Granular soil trough model; b - Straw granule; c - Straw covered model*

According to the requirements of the simulation test, each of the plow surface simulation model was set to three operating speeds of 0.8 m/s, 1 m/s, and 1.2 m/s, respectively. The simulated working depth was equal to the design depth of 270 mm. The EDEM simulation analysis obtained the resistance change of the plow surface under three speeds.

The response surface analysis of the straw burying rate and the working resistance of the plow surface simulation were carried out by Design-Expert 8.0.6. The response values were Force and Burying rates and the investigation factor were velocity and coordinate of E-point in the plow surface. There were three levels for each factor investigation. The code values of -1, 0, 1 were used to represent speed of 0.8 m/s, 1 m/s and 1.2 m/s, and -1, 0, 1 were used to represent the three plow surfaces: C, B and A plow surface, respectively (Table 6). The response surface model (Fig.8) was carried out.

In the case of ensuring the straw burying rate, the working resistance should be as small as possible. The A plow surface has higher burying rate at any of three speeds, but its working resistance was large. The burying rate of the C plow surface was the highest at the speed of 1 m/s, but the working resistance of C was much smaller than that of A. Considering the requirements of forward speed and straw burying rate, the optimal response value was finally determined at (-1,0) point (C plow surface working at speed 1 m/s) could reduce the working resistance while ensuring the burying rate.

**Table 6**

**Coding result of each factor**

| Speed / Type | 0.8 m/s | 1 m/s | 1.2 m/s |
|---|---|---|---|
| **A-plow surface** | (1,-1) | (1,0) | (1,1) |
| **B-plow surface** | (0,-1) | (0,0) | (0,1) |
| **C-plow surface** | (-1,-1) | (-1,0) | (-1,1) |

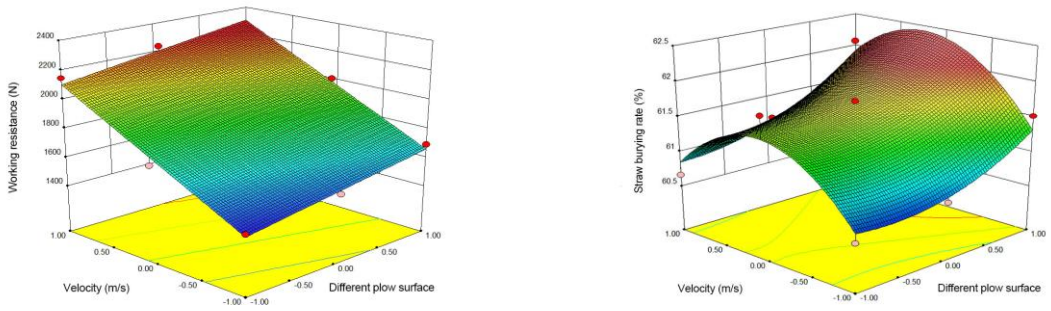


*a - Working resistance* *b - Straw burying rate*

**Fig. 8 - Response surface graph of working resistance and straw burying rate**

**Design of the rotary component**

The cutting pitch, the rotation speed, the radius of rotary blades and the arrangement of the rotary blades on the cutter shaft were key parameters in the design of the rotary component *(Zhou et al., 2001)*. In order to make the machine work stably, the rotary component was arranged in an offset manner. The width of the short-axis side was equal to half of the working width of the plowing component, which was 1000mm. Considering the existence of straw and roots in actual operation, the working width of the rotary component was determined as 2500 mm. The turning direction was confirmed to be forward rotation (Fig.9). According to the design requirements of the machine, the rotary depth *h* was 10 to15 cm.

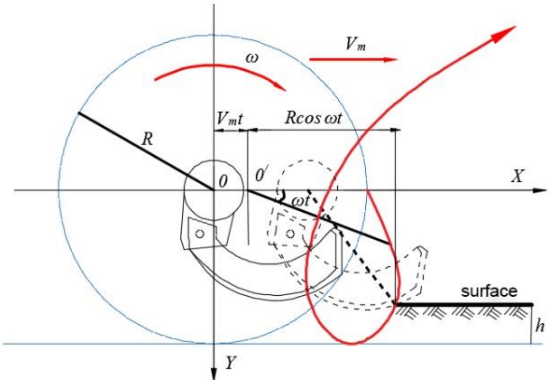


**Fig. 9 - Schematic diagram of rotary blade trajectory**

***Determination of the cutting pitch***

In the time interval between two adjacent blades in the same vertical plane, the forward distance of the rotary machine was called the cutting pitch, which was calculated according to the equation (9).

$$S = V_m \times \Delta t = \frac{2\pi V_m}{n \times \omega} = \frac{2\pi R}{n\lambda} \quad (9)$$

where: *n* is the number of rotating blades installed in the same horizontal plane of the rotary cutter shaft;

*R* is the radius of the cutter shaft rotation;

*λ* is the rotating speed ratio;

*ω* is the angular velocity of the cutter shaft;

$V_m$ is the forward speed of the machine.

***Determination of the rotation speed and the radius of rotary blades***

The range of commonly used rotary speed ratio was from 4 to 10. In this study, the rotary ratio was chosen to be 6, and the relationship between the radius of rotary blade *R* and the rotary ratio *λ* was as follows:

$$R = \frac{nS\lambda}{2\pi} = \frac{100\lambda}{\pi} \quad (10)$$

The rotation radius and theoretical depth of the rotary blade were 195 mm and 100 mm, respectively. The soil surface was uneven after plowing, so the depth of the rotary component was set as slightly less than 100 mm. Considering the rotary ratio and the size of the rotary blade, the rotational angular velocity of the rotary cutter shaft (ω) was determined as follows:

$$\omega = \frac{V_m \lambda}{R} \quad (11)$$

The rotational angular velocity of the rotary cutter shaft was calculated to be 31 rad/s and the rotational speed was 300 r/min so the transmission ratio of the rotary component was 0.56.

***Design of the rotary blades arrangement on the cutter shaft***

Combining agronomic requirements, the blade rest spacing was set as 68 mm and the total number of rotary blades was 73.5 calculated by equation (12). Since the intermediate transmission mode was applied in the machine, the actual rotation width was slightly smaller than the theoretical value. Finally, the total number of rotary blades was rounded to an even number, namely 72.

$$Z' = 1000BZ / b' = (1000 \times 2.5 \times 2) / 68 = 73.5 \approx 72 \quad (12)$$

where: *B* is the working width, m;

*b'* is the tool apron spacing, mm;

*Z* is the number of blades per cutting plane;

*Z'* is the total number of rotary blades.

The arrangement of the rotary blades in this study was 4n±2 *(Feng, 1985)*. Since the right cutter shaft was long, the number of rotary blades for the left and right cutter shaft was 30 and 42, respectively.

***Finite element analysis of the rotary cutter shaft***

Finite element analysis of the rotary cutter shaft was carried out. The stress, displacement and strain were analyzed to verify if the cutter shaft met the job requirements. The rotary cutter shaft was a thin-walled cylinder with an outer diameter of 73 mm and an inner diameter of 63 mm and the simulation parameters were shown in Table 7.

**Table 7**

**Simulation parameters of the cutter shaft**

| parameter | material | Density | Elastic Modulus | Poisson ratio | Yield stress | Torque |
|---|---|---|---|---|---|---|
| Value | Q235 | 7850 kg/m$^3$ | 206 GPa | 0.3 | 235 MPa | 504 N/m |

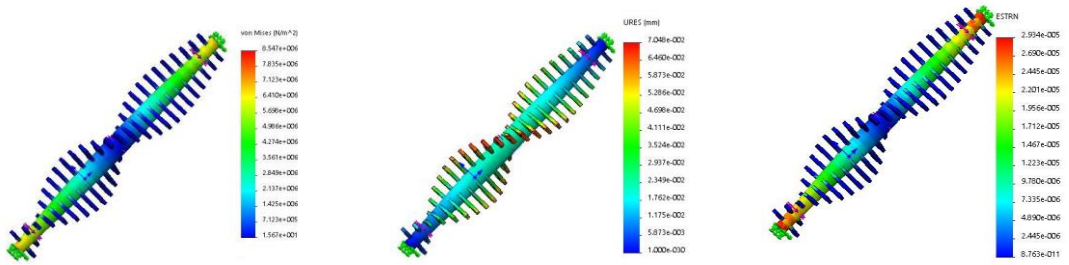

*a - Stress analysis* *b - Displacement analysis* *c - Strain analysis*

**Fig. 10 - Static analysis results of the cutter shaft**

Figure 10 showed that the stress and strain at the ends of the cutter shaft were 8.547MPa and $2.934\times10^{-5}$ respectively, which were the largest. The maximum displacement deformation was in the middle position, which was $7.048\text{x}10^{-2}$ mm. The finite element analysis results showed that the design of the cutter shaft met the strength requirements, which could ensure the normal and stable operation of the rotary component.

## PERFORMANCE TEST

The performance tests and production verification of this combined machine were conducted at the Golden Manor Family Farm in Zhuji Village, Shandong Province (119°53'E, 36°07'N). The measurements included the soil bulk density (g/cm$^{-3}$), soil-breaking rate (%), straw burying rate (%), surface roughness (cm) and fuel consumption (kg/ha). The soil-breaking rate is the percentage of mass of the clods' diameter below 40 mm to the total mass. The surface roughness is the surface fluctuation degree relative to a reference surface, expressed by standard deviation *(Li N., 2012)*.

An X-1204 wheel tractor (88.2kw) was used in the test and the working speed was 3.6 km/h. In the test plot, the soil was loam soil and PH, total porosity, water content and straw coverage were 7.08, 51.59%, 28.5% and 5.5 kg/m$^2$, respectively. For measuring the soil bulk density, a wreath knife was used to take 0-10 cm, 10-20 cm and 20-30 cm soil samples and drying them, measuring soil bulk density before and after the operation. For measuring the soil-breaking rate, all the tillage soil in an area of 0.5 m × 0.5 m was collected. Simultaneously the clod sizes were divided into three levels of less than 4 cm, 4~8 cm and > 8 cm. For measuring the straw burying rate, five 0.5 m x 0.5 m areas were selected in the test plot. All the straw in each of the 0.25m$^2$ area was collected, weighed respectively and an average was taken. For measuring the surface roughness, two stakes were inserted on both sides of the working width, and a horizontal reference line was taken on the stake. The horizontal reference line was equally divided into 5 parts and the distance of each aliquot point to the surface was measured. For measuring the fuel consumption, a CTM-2009 field agricultural machine multi-function tester was applied.

*(a) Straw burying rate* *(b) Fuel consumption*

**Fig. 11 - Field test measurement**

## RESULTS

The bulk density of each soil layer had a decreasing trend after operation (Table 9). Compared with the un-operated soil, the soil bulk density was decreased by 38.06%, 39.13% and 35.90% at 0-10 cm, 10-20 cm, 20-30 cm layer respectively. The machine could reduce soil bulk density and soil compaction, which made the soil looser and was conducive to the subsequent planter operation.

The Chinese national standard and related combined machine operation parameters are shown in Table 10.

**Table 8**

**Measurement results of soil bulk density before and after operation**

| **Depth [cm]** | 0-10 | 10-20 | 20-30 |
|---|---|---|---|
| **Before test [g·cm$^{-3}$]** | 1.55 | 1.61 | 1.56 |
| **After test [g·cm$^{-3}$]** | 0.96 | 0.98 | 1 |

**Table 9**

**Measurement results of soil-breaking rate, straw burying rate and surface roughness**

| **Parameters** | Soil-breaking rate [%] | Straw burying rate [%] | Surface roughness |
|---|---|---|---|
| **Value** | 96.08 | ≥91 | 0.564 |

**Table 10**

**Field test operation parameter standard for related equipment**

| **Parameters** | Moldboard plow | Rotary tiller | Related combined machine |
|---|---|---|---|
| **Soil-breaking rate [%]** | ≥65 | ≥60 | ≥90 |
| **Straw burying rate [%]** | ≥85 | — | ≥90 |
| **Surface roughness [cm]** | — | ≤5 | ≤2 |

The measurement results of soil-breaking rate, straw burying rate and surface roughness were shown in Table 10. The soil-breaking rate reached 96.08%, which was much higher than the national standard of 65%, and was about 6% higher than the related combined machine. It indicated that the plowing component of the combined machine was well coupled with the rotary component.

The straw burying rate in all tests exceeded the requirement (≥90%) stipulated in the Chinese national standard, which indicated that the use of the combined machine could promote the straw returning and reduce the straw burning.

The average of surface roughness was 0.564, which was lower than the national standard of rototiller and related machines.

The average fuel consumption of the plowing and rotary tillage combined machine was measured to be 43.41 kg/ha, which was 16% lower than the average fuel consumption level of Shandong Province *(Wu, 2012)*.

In this study we reached the result that the machine could provide certain technical support for China's straw returning.

## CONCLUSIONS

1. The plowing and rotary tillage combined machine can bury the straw, break the soil and prepare the soil for planting in one operation, which helps promote straw returning and reduce straw burning.

2. The key parameters in this design are the Z-axis value of the intersection E of the side line (EF) and the top edge line (DE). By changing the Z-axis of the point E, different plow surfaces were formed. The orthogonal test results showed that the C-plow surface has the best burying effect at 1m/s.

3. Using the field tests, the effect of the joint operation of the plow component and the rotary component was confirmed. The main performance of the machine such as the soil-breaking rate, the straw burying rate and the surface roughness can meet the related national standards.

**ACKNOWLEDGEMENT**

This study was financially supported by the Special Fund for Agro-scientific Research in the Public Interest from the Ministry of Agriculture, China (Grant No. 201503136) and Innovative Research Team in the University of China (Grant No. IRT13039).

**REFERENCES**

[1] Chang, Z.Z., Wang, D., Yang, S., Wang, C., Zhang, S., (2014), Thoughts on returning straw to field *(对稻麦秸秆还田问题的思考)*, *Jiangsu J. Agric. Sci*. 30, 304–309, Nanjing/ P.R.C.

[2] Feng P.Z., (1985), Optimal arrangement of rotary tiller blades *(旋耕机刀片的最佳数列排列)*, *Journal of Jiangsu Teachers University of Technology*, Changzhou/P.R.C.

[3] Jia H.L., Ma C.L., (2007), Tong J. Study on Universal Blade Rotor for Rototilling and Stubble-breaking Machine [J]. *Soil & Tillage Research*, 94(1): 201-208, Amsterdam/ Netherlands

[4] Kornei T., Istvari J.J., Abdul M.M., (2013), Modelling soil-sweep interaction with discrete element method, *Soil & Tillage Research*, 134 :223-231, Amsterdam/ Netherlands

[5] Lenaerts B., Aertsen T., Tijskens E., et al, (2014), Simulation of grain-straw separation by discrete element modeling with bendable straw particles, *Computers and Electronics in Agriculture*, 101:24-33, Oxford/U.K.

[6] Li H., et al., (2018), Current status and environment impact of direct straw return in China's cropland–A review. *Ecotoxicology and Environmental Safety*, 159: p. 293-300, San Diego/U.S.A.

[7] Li N., (2012), The study on method of evaluation for rotary tiller applicability (*旋耕机适用性评价方法研究*), *Henan Agricultural University*, Zhengzhou/ P.R.C.

[8] Lin J., Zhang T.J., Chen B., Han W., Lv Q.L., Wang J.Q., (2019), Design and test of the combined subsoiling stalk-stubble breaking rotary and ridge machine *(深松灭茬旋耕起垄联合作业机设计与试验)*, *Transactions of the Chinese Society for Agricultural Machinery*, (02):28-39, Beijing/P.R.C.

[9] Wu J.T., (2012), Study on fuel consumption of maize mechanical production in northern China's major producing area *(北方玉米主产区机械化生产燃油消耗研究), China Agricultural University*, Beijing/ P.R.C;

[10] Xie Y.F., Xun J.P., Li C.B., (2009), Current status and development trend of domestic and foreign farming machinery *(国内外耕作机械的现状及发展趋势)*, *Journal of Agricultural Mechanization Research*, (11):238, Harbin/ P.R.C.

[11] Ucgul M., JohnM F., Chris S., (2014), 3D DEM tillage simulation validation of a hysteretic spring (plastic) contact model for a sweep tool operation in a cohesionless soil, *Soil & Tillage Research*, 144: 105-117,220-227, Amsterdam/ Netherlands

[12] Yang H.S., Zhou J.J., Feng J.X., Zhai S.L., Chen W.P., Liu J., Bian X.M., (2018), Ditch-buried straw return: A novel tillage practice combined with tillage rotation and deep ploughing in rice-wheat rotation systems, *Advances in Agronomy*, Volume 154, Pages 257-290, San Diego/U.S.A.

[13] Zeng, M.X., Wang, R.F., Shi-Qi, P., Zhang, Y.J., Cui, Y., Shan, X.Z., Liao, C.Z., Tian, Y.G., (2002), Summary of returning straw into field of main agricultural areas in China*(我国主要农区秸秆还田试验总结)*. *Chinese Journal of Soil Science*,33 (5), 336–339, Shenyang/P.R.C.

[14] Zeng X.Y., MA Y.T., MA L.R., (2007), Utilization of straw in biomass energy in China, *Renewable and Sustainable Energy Reviews*, 11(5): 976-987, Oxford/U.K.

[15] Zhou H.M., Xue W., Sang Z.Z., (2001), Optimized Design Model for General Parameters of a Rotary Tiller *(旋耕机总体参数的优化设计模型)*. *Transactions of the Chinese Society for Agricultural Machinery*, (05):37-39+43, Beijing/P.R.C.